Chapter 2

Numerical Experiments on Turbulent Forced Convection using Low-Reynolds-Number Two-Equation Models

Main contents of this chapter are published as
R. Cònsul, C.D. Pérez-Segarra, J. Cadafalch and K. Claramunt. Numerical experiments on turbulent forced convection using low-Reynolds-number two-equation models. *In Proceedings of the Fifth ECCOMAS Computational Fluid Dynamics Conference*, Barcelona, 2000.

Abstract. The aim of this work is to perform numerical experiments on finite volume computations of turbulent forced convection using different low-Reynolds-number two-equation k-ϵ models. Studied is the performance of these models when predicting different physical phenomena: normal boundary layers, flow with recirculations, impinging flow... To do so, five common test cases of the technical specialized literature corresponding to two dimensional and axisymmetric flows have been selected: flow through a channel, impinging slot jet, flow downstream of a backward facing step, straight pipe flow and axisymmetric sudden expansion. Special emphasis is given on the verification of the computed results by means of an evaluation of the numerical error and the order of accuracy of the solutions. The numerical results are also compared to the experimental data available for each one of the test cases.

2.1 Introduction

The modeling of thermal and fluid-dynamic phenomena involving turbulent forced convection is a key aspect in the design and optimization of many systems of technological interest: heat exchangers, ventilation of buildings, aerodynamics... Nowadays, and due to the increase of the computational capabilities and the improvement of the numerical methods, advanced turbulence models such as DNS (Direct Numerical Simulations) and LES (Large Eddy Simulations) present an encouraging future. Nevertheless, and for practical engineering calculations, RANS (Reynolds Average Navier-Stokes Simulations) and the two-equation turbulent models in particular [1], are still the most popular. In fact, an important effort is still being carried out by many investigators so as to improve the capabilities of these models [2] [3].

The aim of this work is to perform numerical experiments on finite volume computations of turbulent forced convection using different low-Reynolds-number two-equation k-ε models of Jones and Launder [4], Launder and Sharma [5], Ince and Launder [6] and Chien [7]. Studied is the performance of these models when predicting different physical phenomena: normal boundary layers, flow with recirculations, impinging flow... To do so, five common test cases of the technical specialized literature corresponding to two dimensional and axisymmetric flows have been selected: flow through a channel, impinging slot jet, flow downstream of a backward facing step, straight pipe flow and axisymmetric sudden expansion. Special emphasis is given on the verification of the computed results by means of an evaluation of the numerical error and the order of accuracy of the solutions. The numerical results are also compared to the experimental data available for each one of the test cases.

2.2 Mathematical Formulation

The time-averaged governing equations of the fluid flow (continuity, momentum and energy) in two-dimensional Cartesian coordinates, neglecting body forces, heat friction, influence of pressure in temperature, radiation effects, and assuming constant fluid properties and fluid Newtonian behaviour, may be written in tensor notation as:

$$\frac{\partial u_i}{\partial x_i} = 0 \tag{2.1}$$

$$\frac{\partial(\rho u_i)}{\partial t} + \frac{\partial(\rho u_i u_j)}{\partial x_j} = -\frac{\partial p_d}{\partial x_i} + \frac{\partial \tau_{ij}}{\partial x_j} \qquad (i = 1, 2) \tag{2.2}$$

$$\frac{\partial(\rho T)}{\partial t} + \frac{\partial(\rho u_i T)}{\partial x_i} = -\frac{1}{c_p}\frac{\partial \dot{q}_i}{\partial x_i} \tag{2.3}$$

where:

$$\tau_{ij} = \mu\left(\frac{\partial u_i}{\partial x_j} + \frac{\partial u_j}{\partial x_i}\right) - \rho\overline{u_i' u_j'}; \qquad \dot{q}_i = -\lambda\frac{\partial T}{\partial x_i} + c_p\rho\overline{u_i' T'} \tag{2.4}$$

and x_i is the Cartesian coordinate in the i-direction; t the time; u_i the mean velocity in i-direction; T the mean temperature; p_d the mean dynamic pressure; and ρ, μ, λ, c_p are respectively: density, dynamic viscosity, conductivity and specific heat at constant pressure. The turbulent fluctuating velocity in the i-direction and the turbulent fluctuating temperature are indicated by u_i' and T'.

Eddy-viscosity models, like $k-\varepsilon$ turbulence models, use a phenomenological approach in order to evaluate the turbulent stresses and the turbulent heat flux. By analogy to Stokes's viscosity law and Fourier's law, these terms are written in the form:

$$\rho\overline{u_i' u_j'} = -\mu_t\left(\frac{\partial u_i}{\partial x_j} + \frac{\partial u_j}{\partial x_i}\right) + \frac{2}{3}\rho k\delta_{ij}; \qquad \rho\overline{u_i' T'} = -\frac{\mu_t}{\sigma_t}\frac{\partial T}{\partial x_i} \tag{2.5}$$

where: μ_t and σ_t are respectively the turbulent viscosity and the turbulent Prandtl number, and δ_{ij} is the Kronecker delta. The turbulent Prandtl number is usually taken as a constant (a value of 0.9 has been considered in this work). The turbulent viscosity is related to the turbulent kinetic energy (k) and its dissipation (ε) by means of the empirical expression of Kolmogorov-Prandtl. The turbulent kinetic energy and its dissipation are obtained from their transport equations. Although the exact form of these equations results from the Navier-Stokes equations, empirical approximations of some terms are necessary. The resulting $k-\varepsilon$ equations, together with the Kolmogorov-Prandtl expression, can be written, after taking low-Reynolds-number effects into account, as:

$$\mu_t = c_\mu f_\mu \frac{\rho k^2}{\tilde{\varepsilon}} \tag{2.6}$$

$$\frac{\partial(\rho k)}{\partial t} + \frac{\partial(\rho u_i k)}{\partial x_i} = \frac{\partial}{\partial x_i}\left[\left(\mu + \frac{\mu_t}{\sigma_k}\right)\frac{\partial k}{\partial x_i}\right] + P_k - (\rho\tilde{\varepsilon} + D) \tag{2.7}$$

$$\frac{\partial(\rho\tilde{\varepsilon})}{\partial t} + \frac{\partial(\rho u_i\tilde{\varepsilon})}{\partial x_i} = \frac{\partial}{\partial x_i}\left[\left(\mu + \frac{\mu_t}{\sigma_\varepsilon}\right)\frac{\partial\tilde{\varepsilon}}{\partial x_i}\right] + \left(c_{\varepsilon 1} f_1 P_k + E - c_{\varepsilon 2} f_2 \rho\tilde{\varepsilon}\right) T_t^{-1} \tag{2.8}$$

where $\tilde{\varepsilon}$, defined as $\tilde{\varepsilon} = \varepsilon - D/\rho$, is introduced for computational convenience in order to obtain a zero value of $\tilde{\varepsilon}$ at the wall, T_t is the realizable time scale [8] and P_k is the production of turbulence kinetic energy described as:

$$P_k = -\rho\overline{u_i' u_j'}\frac{\partial u_i}{\partial x_j} \tag{2.9}$$

The boundary conditions and the empirical values (c_μ, $c_{\varepsilon 1}$, $c_{\varepsilon 2}$, σ_k, σ_ε, f_1, f_2, f_μ, D and E) depend on the turbulence model adopted. In this work, different models have been employed: Launder and Sharma[5], Jones and Launder[4], Chien[7], Ince and Launder[6]. Hereafter they will be called as LS, JL, CH and IL respectively.

2.3 Numerical Aspects

2.3.1 Numerical Method

The governing equations are discretized on rectangular or cylindrical staggered grids using the finite-volume technique with fully implicit temporal differentiation. The SIMPLEC algorithm is used to couple the discretized equations[9]. The high order scheme SMART is used for the evaluation of the convective terms of the momentum and energy equations, while the convective terms of the turbulent quantities equations are computed using the exponential scheme. On the other hand, the diffusive terms are always evaluated by means of second order central differences. A pressure outflow boundary condition, which allow to reduce the computational domain to that confined within the zones of interest, has been adopted [10]. The resulting set of algebraic equations are solved by means of multigrid solvers [11].

2.3.2 Verification of the computations

In order to asses credibility to the numerical solutions presented in this work, a post-processing tool for the estimation of the numerical error and the order of accuracy has been used. An h-refinement treatment is adopted: the problem is solved on different meshes related by a mesh ratio r (in this work r=2 and five levels of refinement are studied). According to the Richardson extrapolation, with three solutions of a problem obtained on three fine enough consecutive levels of refinement, the order of accuracy of the solutions can be determined.

A map of the estimated order of accuracy is calculated with each three consecutive mesh levels. Thus, as five levels of refinement are used, three order of accuracy maps are obtained.

A high quality solution using a very fine grid and high order numerical schemes is calculated for each one of the test cases, and it is considered the reference solution.

Maps of differences between each refinement level and the corresponding reference solution are carried out, obtaining an estimation of the local numerical error.

The average order of accuracy and the averaged error have been adopted as global estimators of the global order of accuracy and the global numerical error. The post-processing procedure is applied segregately on all the dependent variables of the problem obtaining an estimation of the global order of accuracy and numerical error for each one of them.

More details about this post-processing procedure can be found in [12].

2.4 Test Cases

The aim of this work is to analyze the numerical response of different turbulence models under different turbulent air (Pr=0.71) flows. The models are applied to two simple benchmark situations, a channel and a straight pipe, and to three complex turbulent air flows confined within rectangular and cylindrical geometries: a backward facing step flow, a single turbulent impinging jet and an axisymmetric sudden expansion. Main interest of the two simple benchmark situations is that semi-analytical expressions of the velocity profiles within the wall layer (log-law) and correlations for the skin friction factors and the Nusselt numbers are available. Therefore, results from the computations can be validated by comparison to detailed semi-analytical and experimental data. Concerning the three other cases, some experimental information is also available, and although their geometry is rather simple, the physical phenomena occurring in them involve stagnation and recirculation zones providing strengthen conditions for testing turbulence models.

2.4.1 Channel flow

The developed air flow within a channel of length L and height H with a Reynolds number of $Re_{D_h} = 10^5$ has been considered. Details on the computational domain and the boundary conditions adopted are given in Fig. 2.1. The inlet and the outlet have been modeled by a plug-flow boundary condition and a fixed pressure (p_0) boundary condition respectively. In order to asses a fully developed flow independent from the inlet boundary condition assumed, a geometry ratio between the domain length L and the hydraulic diameter D_h of $L/D_h = 60$ has been adopted. The computational domain has been limited to the lower half part of the channel, considering a symmetry boundary condition at the top side, and an isothermal wall, at a temperature of T_w, at the bottom side.

Non-uniformly distributed meshes of n*n control grid nodes have been use (levels of refinement: n=10, 20, 40, 80 and 160). A concentration tanh-like function with a

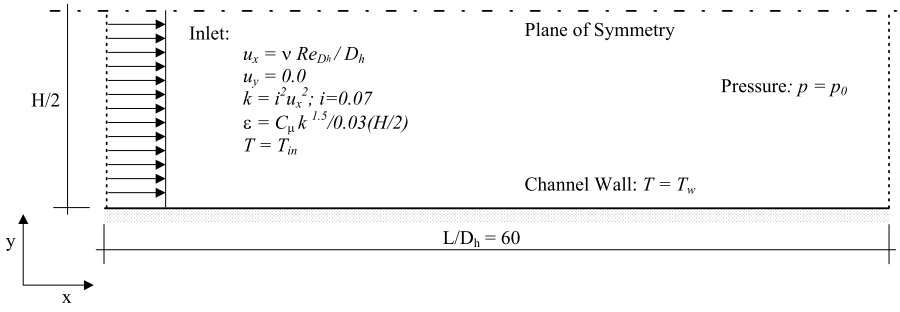

Figure 2.1: Channel flow. Computational domain the boundary conditions.

concentration factor of 1 in the x-direction intensified at the inlet, and with a factor of 4 in the y-direction intensified at the wall are considered.

Computation results are compared to the semi-analytical expression for the u-velocity profile at the logarithmic layer, to the friction factor values C_f from the experimental correlation of Özisik [13], and to the Nusselt numbers Nu from the correlation of Dittus-Boelter:

$$u^+ = 2.5 \ln(y^+) + 5.5 \tag{2.10}$$

$$\frac{1}{\sqrt{C_f}} = 2.0 \log Re_{D_h} \sqrt{C_f} - 0.8 \tag{2.11}$$

$$Nu = 0.023 Re_{D_h}^{0.8} Pr^{0.4} \tag{2.12}$$

2.4.2 Flow downstream of a backward facing step

In this second test case, the flow downstream of a backward facing step has been studied. Boundary conditions and the computational domain are described in detail in Fig. 2.2. A fully developed flow over a flat plate has been considered at the inlet with $Re_H = 2.8 * 10^4$ and with constant temperature T_{in}. At the outlet, a pressure boundary condition has been imposed. The left side wall has been fixed at a constant temperature of T_{in}, and a heat flux $q_w = 270 W/m^2$ has been imposed at the bottom wall. Main stream values have been considered far enough from the wall.

The case has been computed also over non-uniformly distributed meshes (five refinement levels: n=10, 20, 40, 80 and 160). Distributions of tanh-like functions have

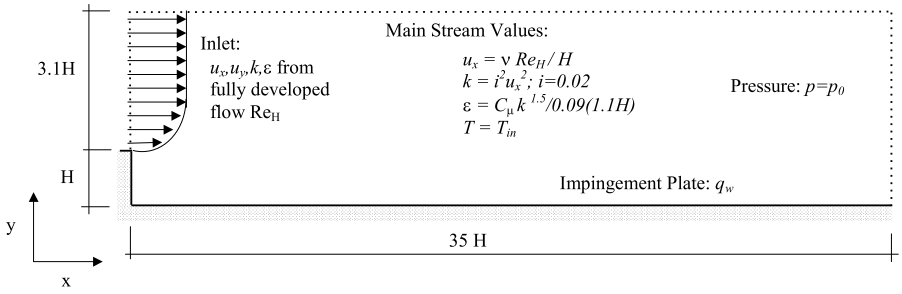

Figure 2.2: Flow downstream of a backward facing step. Computational domain and boundary conditions.

been used considering intensification factors of 4 near the walls. The recirculation zone has been discretized uniformly and decreasing the mesh density to the outlet. The domain is discretized using n grid nodes in the y-direction at the inlet, $0.4n$ grid nodes in the y-direction at the side wall, and $1.8n$ grid nodes in the overall x-direction. For example, for the fourth level of grid refinement n=80, an overall number of grid nodes of $112 * 144$ have been used.

Numerical results have been compared to the experimental data of Adams et al. [14] and Vogel and Eaton [15].

2.4.3 Impinging slot jet flow

The third test case consists of a slot jet flow with $Re_W = 10^4$ impinging a flat plate. See Fig. 2.3 for details on the boundary conditions and computational domain. The structure of the turbulent flow is computed considering two parallel plates at different temperatures with a flow entrance at the top plate. The flow enters into the domain perpendicular to the parallel plates. Due to the domain symmetry characteristics, only half channel with symmetry boundary conditions is calculated.

The computational domain has been discretized using n grid nodes in the y-direction and $1.7n$ in the x-direction over five levels of refinement: n=10, 20, 40, 80 and 160. Therefore, a mesh of n=80 means $136 * 80$ nodes. Near the walls the grid has been concentrated by means of a tanh-like function with a concentrator factor of 2. Concerning the x-direction, the stagnation region has been discretized regularly, and the outer region (from the stagnation region to the outlet) decreasing the grid density when approaching the outlet.

Numerical results have been compared to experimental data of Van Heiningen[16].

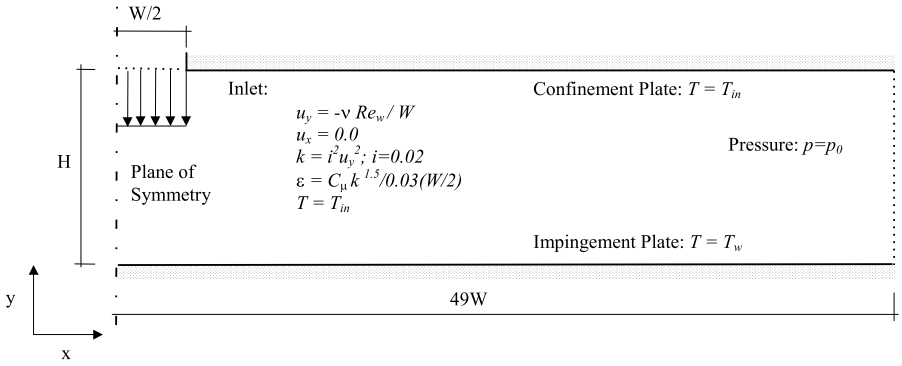

Figure 2.3: Impinging slot jet flow. Computational domain and boundary conditions.

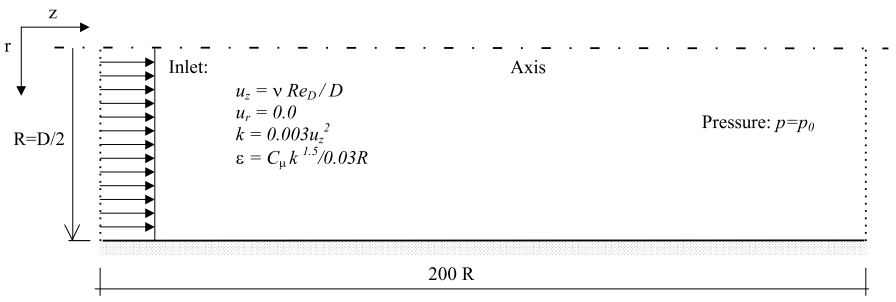

Figure 2.4: Pipe flow. Computational domain and boundary conditions.

2.4.4 Pipe flow

Fully developed turbulent flow with $Re_D = 4 * 10^4$ within a pipe of length L and diameter D=2R. Details on the axisymmetric computational domain and the boundary conditions adopted are given in Fig. 2.4. In order to assure fully development of the flow, a geometry ratio of $L/D = 100$ has been adopted.

A mesh of $n * n$ number of grid has been used, intensifying the grid in the axial direction at the inlet and in the radial direction at the wall by means of a tanh-like function with a concentrator factor of 1 and 4 respectively.

Computed results have been compared to the experimental data given by Laufer[17].

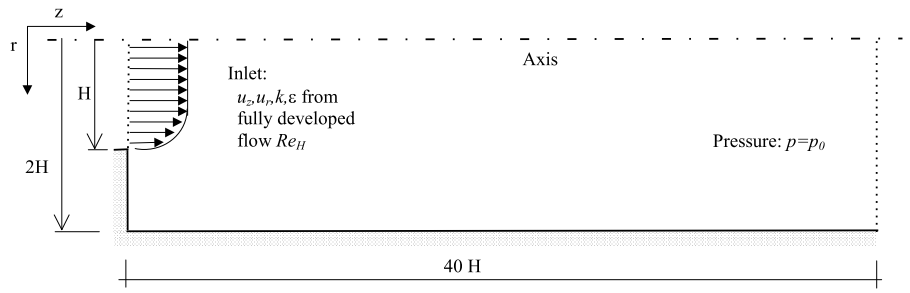

Figure 2.5: Axisymmetric sudden expansion. Computational domain and boundary conditions.

2.4.5 Axisymmetric sudden expansion

The separated flow following a sudden expansion in axisymmetric configurations has both theoretical and practical importance since it involves a complex phenomena and is found in a wide variety of important applications (e.g. combusters). Furthermore, due to the axial symmetry of the flow, axisymmetric computations can be compared to experimental measurements with a high level of accuracy.

The computed test case is based on the experimental studies carried out by Gould et al. [18] for a Reynolds number of $Re_H = 4.7 * 10^4$. In Gould's set-up, two tubes with different diameters where connected with a nozzle and forcing the expansion after it. Details on the axisymmetric computational domain and the boundary conditions adopted are given in Fig. 2.5. The inner tube radius is H and the outer tube radius is $2h$ (i.e. the step size is H). Fully development of the flow after the reattachment point has been assured using a computation domain length forty time the step size H. As a first attempt to reproduce numerically the experimental results of Gould et al., fully development of the flow before the expansion has been considered. However, there are some discrepancies between this assumption and the conditions imposed at the set-up of Gould et at.

The grid employed in terms of the grid parameter n, is similar to that used in the test case flow downstream of a backward, being the five levels of grid refinement n=16, 32, 64, 128 and 256.

2.5 Results

This section is divided into two parts. In the first part some of the data obtained from the verification process applied to each one of the solutions is given. The second

part encompasses physical data such as Nusselt numbers Nu, velocity profiles and friction factors, C_f, compared to available experimental and semi-analytical values. They can be useful for further comparison to solutions of other numerical codes or future versions of the numerical code here used, and for benchmarking purposes in general.

2.5.1 Results from the verification process

Much information is obtained from the verification process for each one of the dependent variables of the problems: local and global estimates of the order of accuracy, local and global estimates of the numerical error, classification of the computational nodes according to how the solution converges with the mesh refinement... This large amount of data is difficult to be given in a paper like this in a clear manner. Fortunately, similar results from the verification have been obtained for each test case when study different turbulence models and dependent variables (temperature or velocity components). Therefore, only some of the data corresponding to one of the dependent variables, x/axial-component of the velocity field, and for solutions obtained with one turbulence model will be given for each test case. These data are the evolution with the mesh refinement of the average absolute discretization error normalized by the entrance velocity $\overline{e_D^*}$, and of the observed averaged order of accuracy $\overline{p}$.

As already commented in previous sections, all solutions have been obtained on a h-refinement procedure over five levels of refinement represented by the parameter n. As described in section 2.4, the parameter n does not mean for all the tested cases that the number of grid points used is $n * n$. For example, in the impinging slot jet flow solutions, the number of grid points in terms of n is $1.7n * n$.

For the evaluation of the discretization error $\overline{e_D^*}$ the solutions with the finest mesh, and with the high order numerical scheme SMART has been used as reference solution.

For discussion purposes, verification data here presented is compared to that obtained when using the first order accurate UDS scheme to approximate the convective terms of the momentum equations.

The data corresponding to the channel flow case are given in Fig. 2.6a and Table 2.1a. The five levels of refinement correspond to n=10, 20, 40, 80 and 160. Due to the one-dimensional nature of the flow structure, diffusive terms are predominant. Therefore, as observed in Table 2.1a, the order of accuracy tends to the formal order of accuracy of the central difference scheme used for the diffusive schemes whatever numerical scheme is used for the convective terms of the momentum equation, i.e. $p = 2$. As it can be observed in Fig. 2.6a, the average absolute discretization error is decreased by a factor of around 4 between two consecutive levels of refinement, and normalized errors below 0.2% are predicted for n=80 and 160.

The estimated values for the discretization error and the order of accuracy corresponding to the solutions of the flow downstream of a backward facing step are

grid	$\overline{p}$	
n	UDS	SMART
40	1.33	1.11
80	1.73	1.68
160	1.83	1.89

(a)

grid	$\overline{p}$	
n	UDS	SMART
40	-	0.77
80	1.20	1.31
160	1.30	1.60

(b)

Table 2.1: Average order of accuracy of the u_x-velocity field vs. grid level. (a) Channel flow. Turbulence model: JL. (b) Flow downstream of a backward facing step. Turbulence model: IL.

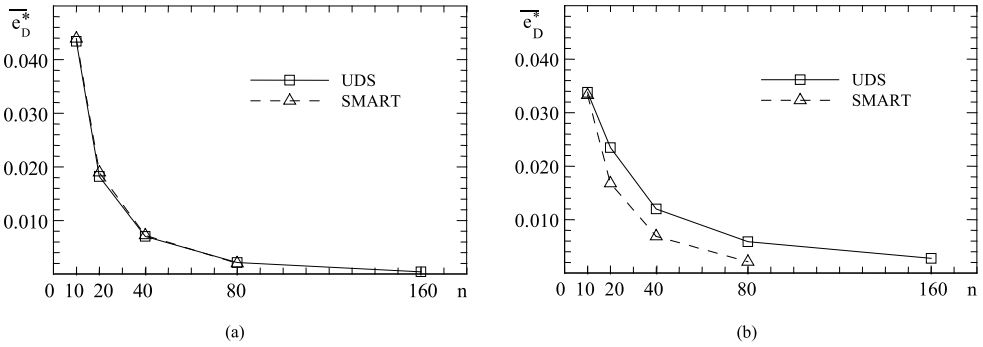

Figure 2.6: Average absolute normalized discretization error of the u_x-velocity field vs. grid level. (a) Channel flow. Turbulence model: JL. (b) Flow downstream of a backward facing step. Turbulence model: IL.

given in Fig. 2.6b and Table 2.1b. In the recirculation zone both convective and diffusive terms characterize the flow, thus, the resulting observed order of accuracy is the result of the effects of the numerical schemes used for both terms. Therefore, higher observed order of accuracy are computed for the solutions using SMART (with a theoretical order of accuracy between 1 and 3) than for those using UDS (with a theoretical order of accuracy of 1). Concerning the normalized absolute discretization error, when using the SMART scheme values below 0.2% are obtained for the two finer grid levels, n=80 and 160.

Physical phenomena involved in the pipe flow and the axisymmetric sudden expansion are similar to that of the channel flow and the flow downstream of a backward facing step. In fact they are the same problem in axisymmetric and Cartesian coordi-

grid	$\overline{p}$	
n	UDS	SMART
40	1.10	1.25
80	1.73	1.81
160	1.88	1.90

(a)

grid	$\overline{p}$	
n	UDS	SMART
64	0.60	0.43
128	0.71	0.80
256	1.07	2.35

(b)

Table 2.2: Average order of accuracy of the axial-velocity field vs. level of refinement. (a) Pipe flow. Turbulence model: LS. (b) Axisymmetric sudden expansion. Turbulence model: IL.

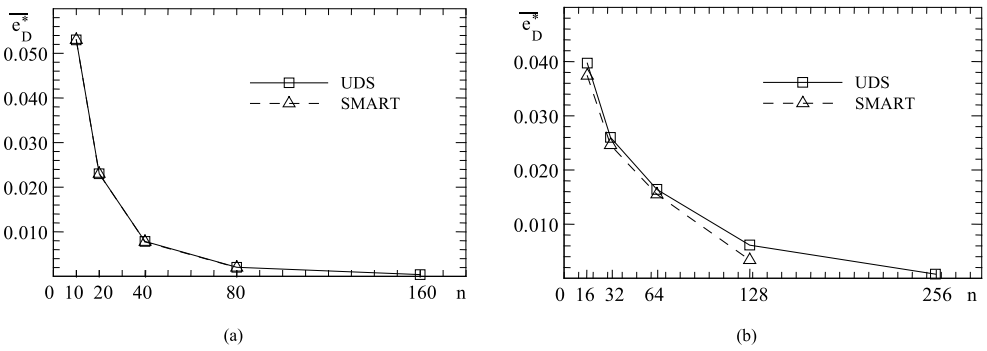

Figure 2.7: Average absolute normalized discretization error of axial-velocity field. (a) Pipe flow. Turbulence model: LS. (b) Axisymmetric sudden expansion. Turbulence model: IL.

nates respectively. Data obtained from the verification process of the solution of the axisymmetric cases are given in Fig. 2.7 and Table 2.2. Some differences respect to the tendencies observed in the corresponding cases with Cartesian coordinates previously discussed are observed, see Fig. 2.6 and Table 2.1. This can be justified by the fact the the Reynolds numbers adopted for the corresponding cases with Cartesian and axisymmetric coordinates are not the same. Nevertheless, reasonable values are also obtained. Values of $\overline{e^*_D}$ for the axial-velocity field are below $0.4 \div 0.2\%$ for the solutions using SMART, and values of $\overline{p}$ approaching the theoretical order of accuracy are found for the finest set of solutions.

Further results regarding the effect of the level of grid refinement on the solutions of the backward facing step case and the axisymmetric sudden expansion case are also given in Table 2.3. Given is the reattachment point calculated using the IL turbulence

grid	reattachment point	
n	UDS	SMART
10	3.20	4.04
20	3.94	4.70
40	4.64	5.11
80	5.08	5.33
160	5.32	5.46

(a)

grid	reattachment point	
n	UDS	SMART
16	8.69	8.77
32	9.65	9.71
64	10.42	10.50
128	11.11	11.32
256	11.47	11.51

(b)

Table 2.3: Reattachment point vs. grid level n. Turbulence model: IL. (a) Flow downstream of a backward facing step. (b) Axisymmetric sudden expansion.

model in terms of the level of refinement represented by the parameter n. Again, for comparison purposes, results computed with UDS scheme for the convective terms of the momentum equations are also given.

Results of the verification process of the solutions of the impinging slot jet were not as successful as those previously presented. The observed order of accuracy did not tend to the expected theoretical values, and the estimated normalized error did not vanish asymptotically with the mesh refinement. A possible explanation of this behaviour is the presence of laminar-turbulent flow that is typically difficult to be handled by the two-equations turbulence models. Therefore, the results for the impinging slot jet flow must be kept in caution, because the verification process is indicating that the discretization levels used may not be enough.

2.5.2 Phenomenological data

Data presented in this subsection correspond to those simulations obtained with the SMART numerical scheme and with the fourth level of refinement for all the cases except to the channel flow, which results correspond to the fifth level of refinement.

Channel flow

Results of the channel flow case are shown in Table 2.4. Given are the computed values of the skin friction coefficients C_f, the Nusselt number Nu, the velocity profile at the logarithmic layer and the normalized turbulent kinetic energy at the symmetry axis of the channel $k^+ = k/u_\tau^2$, where u_τ is the shear velocity. The values of the friction coefficients and the Nusselt number have been compared to those given by the empirical correlation of Özisik and Dittus-Boelter obtaining the relative errors given in Table 2.4 within brackets. All the models considered have a very similar behaviour,

model	$C_f * 10^3$		Nu		k^+	a	b
LS & IL	4.58	(1.7%)	189.65	(−7.9%)	0.904	2.82	3.87
JL	4.62	(2.7%)	188.39	(−8.5%)	0.944	2.98	2.77
CH	4.59	(2.0%)	189.05	(−8.2%)	0.886	2.71	4.51

Table 2.4: Channel flow: skin friction C_f, Nusselt number Nu, normalized turbulent kinetic energy at the symmetry axis of the channel k^+, and a and b coefficients of the log-law $u^+ = a\ln(y^+) + b$. Relative errors of the C_f and Nu respect to the correlations of Özisik and Dittus-Boelter are indicated within brackets.

model	reattachment point		$St_{max} * 10^3$	
LS	4.83H	(−27.5%)	22.7	(611%)
JL	5.33H	(−20.0%)	19.8	(520%)
CH	4.60H	(−31.1%)	9.45	(195%)
IL	5.33H	(−20.0%)	4.32	(35.0%)

Table 2.5: Flow downstream of a backward facing step: reattachment point in terms of the step size H and maximum Stanton number. Comparison to the experimental values from Vogel and Eaton. Within brackets the relative error respect to the experimental values are given.

appearing only small differences between them and having a good agreement to the values obtained from the correlations. The velocity profile at the logarithmic layer is given according to the expression $u^+ = a\ln(y^+)+b$. Coefficients a and b have been calculated by means of the straight line from y^+=100 to y^+=500, i.e. from (ln(100),u^+) to (ln(500),u^+). The best fit to the semi-analytical log-law $u^+ = 2.5ln(y^+) + 5.5$ is provided by the model CH.

Flow downstream of a backward facing step

In Table 2.5 the values of the reattachment point and the maximum value of the Stanton number at the wall are presented compared to the experimental values from Vogel and Eaton. The percentage error respect to these experimental values are also shown. The numerical solutions show a poor agreement with the experimental data for all the turbulence models except for the Ince-Launder (IL) model. In Fig. 2.8, the Stanton number and the skin friction profiles are presented. As it can be seen, only IL model predicts the curve shapes measured by Vogel and Eaton[15] and Adams et

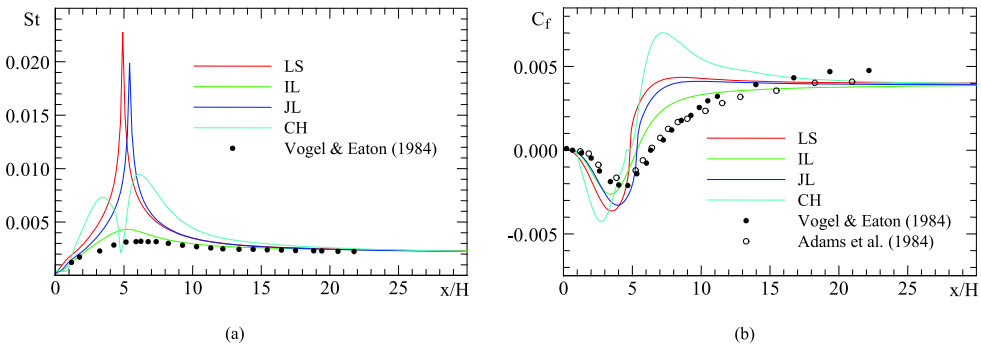

Figure 2.8: Flow downstream of a backward facing step (step size=H). (a) Stanton number vs. x/H. Comparison to the experimental values from Vogel & Eaton. (b) Skin friction vs. x/H. Comparison to the experimental values from Vogel & Eaton and from Adams et al.

al.[14]. A peak value in the Stanton number profile is obtained with LS and JL models in the reattachment point coinciding with near infinite slopes in the corresponding curves of the friction factor. The model CH predicts the presence of two peaks in the St number before and after the reattachment point, and a non-real maximum value of the friction factor coefficient after the reattachment point.

Impinging slot jet flow

Fig. 2.9 shows the Nusselt number and the skin friction profiles at the hottest wall (bottom) considering IL and CH models in comparison to the experimental data obtained by Van Heiningen[16]. The heat transfer rate measured by van Heiningen has its peak value at the center of the impingement, decreasing and having a second lower peak at x=$5W$, where W is the inlet aperture. Although the computations reproduce this global structure, the location of the second peak is predicted for x larger than $11W$. Furthermore, the location of this second peak has been found to be very sensitive to the mesh used, being difficult to find a grid independent solution.

Pipe flow

Main computed features of the pipe flow are given in Table 2.6: the friction factor coefficient C_f, the axial mean-velocity u at the axis normalized by the mean stream velocity u_s, the turbulent kinetic energy normalized by the shear velocity u_τ up to the power of 2, $k^+ = k/u_\tau^2$, and the coefficients of the velocity profile in the logarithmic

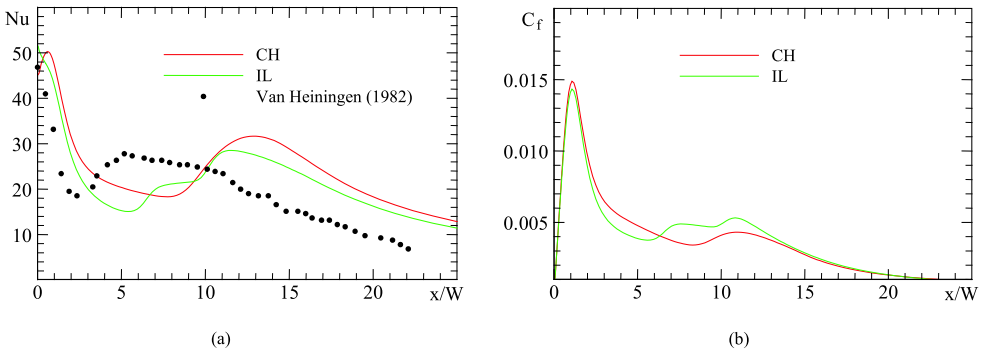

Figure 2.9: Impinging slot jet flow (inlet aperture = W). (a) Nusselt number vs. x/W. Comparison to the experimental values of Van Heiningen. (b) Skin friction vs. x/W.

region according to the log-law expressed as $u^+ = a\ln(y^+) + b$. Coefficients a and b have been calculated from the u^+ values at the points y^+=100 and y^+=500.

When comparing the results of different turbulence models, small discrepancies are found for the skin friction coefficient, the axial mean-velocity at the axis and the turbulent kinetic energy at the axis. More relevant differences appear in the parameters of the log-law, which are always rather different from the semi-empirical parameters of the universal law of the wall a=2.5 and b=5.5.

More detailed data is given in Fig. 2.10 and Fig. 2.11 compared to that of the experimental data of Laufer [17]. Fig. 2.10 shows the axial mean-velocity distribution u normalized by the mean stream velocity u_s as a function of $(R-r)/R$, where R is the radius of the pipe and r the coordinate in the radial direction ($r = 0$ corresponds to the pipe center). The mean-velocity profiles in the wall layer are given in Fig. 2.11b. It can be observed as the mean-velocity calculated with all the turbulence models fit quite well to the experimental values of Laufer. On the other hand, more important discrepancies are observed in the fluctuating velocities. The root-mean-square values of the axial velocity fluctuations near wall are shown in Fig. 2.11a normalized by the shear velocity u_τ. Now, as it could be expected a priori, differences between experimental data and numerical data are important. The components of the fluctuation of velocity when approaching the wall differ. While tangential components grow up near the wall, the perpendicular components tend to drop down. Assumptions made in the two-equations turbulence models avoid these anisotropic effects and, therefore, experimental data cannot be reproduced by the model properly.

model	$C_f * 10^3$	u/u_s	k^+	a	b
LS & IL	5.44	1.19	1.20	2.86	3.66
JL	5.52	1.20	1.27	3.03	2.63
CH	5.52	1.19	1.19	2.74	4.45

Table 2.6: Pipe flow: skin friction C_f, axial mean-velocity u at the axis normalized by the mean stream velocity u_s, normalized turbulent kinetic energy at the axis k^+, and a and b coefficients of the log-law $u^+ = a\ln(y^+) + b$.

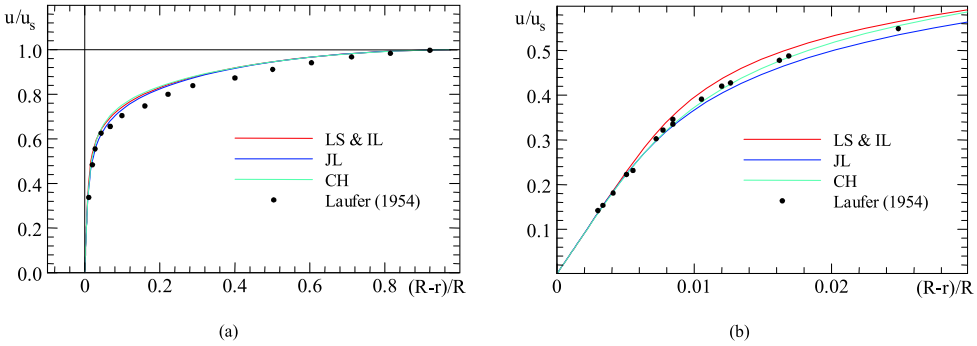

Figure 2.10: Pipe flow. Mean-velocity distribution normalized by the mean stream velocity u_s. (a) Whole distribution. (b) Near-wall values.

Axisymmetric sudden expansion

The last test studied is the axisymmetric sudden expansion. The reattachment point obtained by the different models is indicated in Table 2.7 compared to the experimental data measured by Gould [18]. Important differences respect to the experimental data are found. Further work need to be done in the computation of this case so as to try to reproduce more properly the experimental conditions at the inlet of the computational domain. Differences between the assumption of fully development of the flow at the inlet and the experimental conditions could justify the discrepancies of the predicted reattachment points respect to the experimental value.

2.6 Conclusions

Numerical studies of turbulent forced convection using different low-Reynolds number two-equation models have been presented.

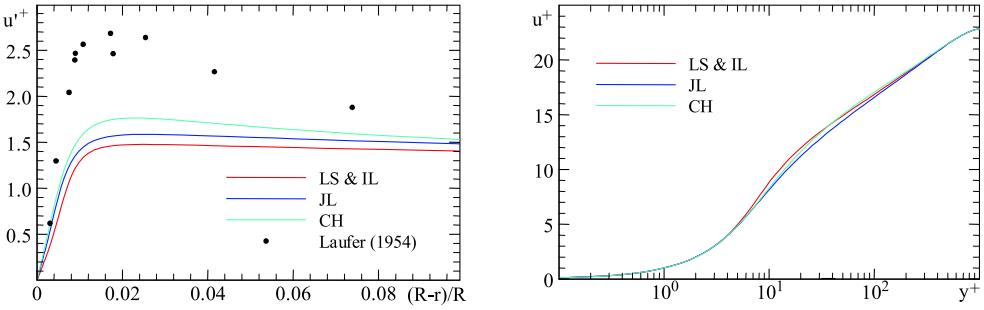

Figure 2.11: Pipe flow. (a) Root-mean-square values of the axial velocity fluctuations near wall normalized by the shear velocity u_τ. (b) Mean-velocity profile in the wall layer: u^+ vs. y^+.

model	reattachment point	
LS	9.29H	(+16.2%)
JL	10.53H	(+31.6%)
CH	12.68H	(+58.5%)
IL	11.32H	(+41.5%)

Table 2.7: Axisymmetric sudden expansion: reattachment point in terms of the step size H. In brackets, the relative error respect to the experimental values of Gould are indicated.

Five common test cases of the technical specialized bibliography have been selected in order to analyze the performance of the different turbulence models considered. The test cases chosen for these studies correspond to two-dimensional and axisymmetric air flows: the flow through a channel, the impinging slot jet, the downstream of a backward facing step , the straight pipe flow, and the axisymmetric sudden expansion.

Numerical results have been verified by means of a post-processing procedure for the estimation of the order of accuracy and the discretization error of numerical solutions obtained on a h-refinement criteria. All numerical results here presented except those corresponding to the impinging slot jet have been shown to be nearly free of numerical errors. Whenever available, numerical solutions have been compared to experimental data from the literature.

For the simpler test cases: channel flow and pipe flow, the differences on the solutions obtained with different turbulence model are not significant and the agreement

with the experimental data is quite good. For the more complex flows (the impinging slot jet, the downstream of a backward facing step and the axisymmetric sudden expansion) more important discrepancies between the models and the experimental data have been observed.

2.7 Acknowledgments

This work has been financially supported by the Comisión Interministerial de Ciencia y Tecnología, Spain (project TIC99-0770).

References

[1] C.D. Pérez-Segarra, A. Oliva, M. Costa, and F. Escanes. Numerical experiments in turbulent natural and mixed convection in internal flows. *International Journal for Numerical Methods for Heat and Fluid Flow*, 5(1):13–33, 1995.

[2] J. Piquet. *Turbulent flows-models and physics*. Springer-Berlag, 1999.

[3] K. Heyerichs and A. Pollard. Heat transfer in separated and impinging turbulent flows. *International Journal of Heat and Mass Transfer*, 39(12):2385–2400, 1996.

[4] W.P. Jones and B.E. Launder. The prediction of laminarization with a two-equation model of turbulence. *International Journal of Heat and Mass Transfer*, 15:301–314, 1972.

[5] B.E. Launder and B.I. Sharma. Application of the energy dissipation model of turbulence to the calculation of flow near a spinning disc. *Letters in Heat Transfer*, 1:131–138, 1974.

[6] N.Z. Ince and B.E. Launder. Computation of turbulent natural convection in closed rectangular cavities. In *Proceedings of the 2nd U.K. Natural Conference Heat Transfer*, volume 2, pages 1389–1400, 1988.

[7] K.Y. Chien. Prediction of channel and boundary layer flows with a low reynolds number 0 model. *AIAA Journal*, 20:33–38, 1982.

[8] U. Goldberg, O. Peroomian, and S. Chakravarthy. A wall-distance-free k-ϵ model with enhanced near-wall treatment. *Journal of Fluids Engineering*, 120:457–462, 1998.

[9] S.V. Patankar. *Numerical heat transfer and fluid flow*. Hemiosphere Publishing Corporation, 1980.

[10] S.R. Marthur and J.Y. Murthy. Pressure boundary conditions for incompressible flow using unstructured meshes. *Numerical Heat Transfer, Part B*, 32:283–298, 1997.

[11] B.R. Hutchinson and G.D.Raithby. A multigrid method based on the additive correction strategy. *Numerical Heat Transfer, Part B*, 9:511–537, 1986.

[12] J. Cadafalch, A. Oliva, C.D. Pérez-Segarra, M. Costa, and J. Salom. Comparative study of conservative and nonconservative interpolation schemes for the domain decomposition method on laminar incompressible flows. *Numerical Heat Transfer, Part B*, 35(1):65–84, 1999.

[13] M.N. Ozisik. *Heat transfer. A basic approach.* McGraw-Hill, 1985.

[14] E.W. Adams, J.P. Johnston, and J.K. Eaton. Experiments on the structure of turbulent reattaching flow. Technical report, Thermosciences Group, 1984.

[15] J.C. Vogel and J.K. Eaton. Heat transfer and fluid mechanics measurements in the turbulent reattaching flow behind a backward-facing step. Technical report, Thermosciences Group, 1984.

[16] A.R.P. Van Heiningen. *Heat transfer under impinging slot jet.* PhD thesis, McGill University, 1982.

[17] J. Laufer. The structure of turbulence in fully 0 flow. Technical report, National Association for Campus Activities, 1954.

[18] R.D. Gould, W.H. Stevenson, and H.D Thompson. Investigation of turbulent transport in an axisymmetric sudden expansion. *AIAA Journal*, 28(2):276–283, 1990.